STEMinar

Journal

Volume 3
September 2017

CU STEMinar

FROM THE EDITOR

I am delighted to assume the position of editor for CU Boulder's Graduate STEMinar Journal as it returns to publication following a brief hiatus. Additionally, STEMinar welcomes a new president, Megan Harries, and vice president, Albany Thompson. It is our hope that STEMinar will continue to foster and support CU Boulder's graduate student community

STEMinar seeks to promote interdisciplinary interaction among STEM graduate students. Bimonthly seminars are hosted throughout the year to give students an opportunity to learn about new areas of research outside of their own field. Since its inception in 2013, STEMinar has hosted speakers from a variety of STEM departments including computer science, mathematics, geology, physics, chemistry, evolutionary biology, psychology and neuroscience, and several engineering sub-disciplines including aerospace and mechanical.

Thanks to a generous contribution from John Stevenson, the Dean of the CU Boulder Graduate School, STEMinar provides multiple graduate student grants. To further our goal of making this research accessible to a broad audience, recipients are asked to contribute a short document summarizing their current research project, or reviewing a STEM topic of interest.

It is my hope that this journal will continue to highlight the ongoing research of STEM graduate students at CU Boulder. The current issue contains the seminar schedule for the upcoming Fall 2017 semester, as well as articles submitted by individuals who received support during the previous grant cycle.

Sincerely,
Louisa Smith
Incoming Editor

Table of Contents:

STEMinar Schedule
Fall 2017

Thursday, September 7th

Welcome and Introductions to new leadership

- ♦ Megan Harries (Chemistry)
- ♦ Albany Thompson (Mathematics)
- ♦ Louisa Smith (Psychology & Neuroscience)

Tuesday, September 19th

Olivia Hirschey, Linguistics

Thursday, October 5th

Mary Bastawrous, Aerospace Engineering

Tuesday, October 17th

Ian Martiny, Computer Science

Thursday, November 2nd

Sarah Salmon, Mathematics

Tuesday, November 14th

Brian Aguado, Chemical and Biological Engineering

Thursday, December 5th

Ben Pollard, Physics Education

Tuesda, December 14th

Aaron Lamplugh, Mechanical Engineering

ANALYSIS OF GROUNDWATER FLOW IN MOUNTAINOUS, HEADWATER CATCHMENTS WITH PERMAFROST

Sarah G. Evans

Department of Geological Sciences
University of Colorado Boulder

ABSTRACT. Headwater catchments have a direct impact on the water resources of downstream lowland regions as they supply freshwater in the form of surface runoff and discharging groundwater. Often, these mountainous catchments contain expansive permafrost that may alter the natural topographically controlled groundwater flow system. As permafrost could degrade with climate change, it is imperative to understand the effect of permafrost on groundwater flow in headwater catchments. This study characterizes groundwater flow in mountainous headwater catchments and evaluates the effect of permafrost in the context of climate change on groundwater movement using a three-dimensional, finite element, hydrogeologic model. The model is applied to a representative headwater catchment on the Qinghai-Tibet Plateau, China. Findings suggest that increased annual air temperatures may increase groundwater discharge to streams, which has implications for ecosystem health and the long-term availability of water resources to downstream regions.

Key words: permafrost, groundwater, modeling, headwater catchment

Contact Information: Sarah.G.Evans@colorado.edu

INTRODUCTION

Headwater catchments play a key role in supplying regional groundwater. In headwater systems, groundwater recharges at high elevations and discharges to valleys, serving as a primary source of freshwater to lowland regions [1]. The effects of climate change are predicted to exacerbate freshwater deficits in lowland regions [2]. This may occur, in part, as groundwater supplies from high latitude and high elevation headwater regions are altered by permafrost degradation [3].

Permafrost is defined as the subsurface region that remains below 0°C for two or more consecutive years [4]. Globally, permafrost occupies expansive portions of the high latitudes and is found intermittently within high elevation areas at lower latitudes. Approximately 24% of the land surface in the northern hemisphere is underlain by permafrost [5]. Estimates suggest that 83% of the high elevation Qinghai-Tibet Plateau in China is underlain by permafrost, making it the largest area of high elevation permafrost in the world [6].

In headwater catchments, permafrost alters groundwater flow paths. Under natural conditions, groundwater flow paths are typically either shallow or deep (Figure 1). The depths of groundwater flow paths are governed by the magnitude of both local and regional topographic slope. When regional topographic slope is steep, regional gradients overwhelm local-scale circulation patterns and flow paths are relatively deep. Shallow flow paths occur within surficial sediment, whereas deep flow paths occur when groundwater percolates into fractured bedrock. In regions without permafrost, the water table is usually a subdued replica of topography (Figure 1), creating topographically controlled, nested, groundwater flow systems (e.g., [7], [8]). In areas with permafrost, permafrost acts as an aquitard, impeding downward groundwater flow while consequently enhancing groundwater–surface water interactions [9].

Figure 1. Schematic diagram illustrating groundwater movement in a headwater catchment (left) without permafrost and (right) with permafrost. Black lines are groundwater flow paths. Grey dashed line indicates low magnitude groundwater flow. The vadose zone is assumed to be relatively thin and is not modeled.

In the last few decades, climate change has perturbed the natural state of headwater catchments by increasing the thickness of the freeze-thaw layer and reducing permafrost areal extent [10], [11]. [12] found that from 1970 to 2000 the areal extent of permafrost on the Qinghai-Tibet Plateau was reduced by approximately 19%. In the future, as climate change is expected to increase regional and global temperatures, rates of permafrost degradation are expected to accelerate [13]. [14] hypothesized that by the end of the 21st century, the areal extent of permafrost on the Qinghai-Tibet Plateau could decrease by 81%.

In some regions such as on the Qinghai-Tibet Plateau, it is suggested that groundwater flow plays a major role in permafrost degradation [6]. Groundwater flow degrades permafrost through a positive feedback cycle that is initiated by warming. As air temperatures increase, permafrost thaws, and the ice in pore spaces melts into liquid water. This leads to more porous

soils with greater permeability, increasing groundwater flow [15]. Increased groundwater flow, in turn, promotes permafrost degradation as warm groundwater flows laterally, and then vertically through, permafrost [16]. This cycle is suggested to promote the release of sequestered carbon that may cause further warming [17].

This study simulates a headwater catchment system with permafrost in order to quantitatively analyze the spatially and temporally variable trend of baseflow and the responses of permafrost and groundwater to warming at the catchment scale. The primary objectives of this study are to (1) examine how permafrost affects groundwater flow paths and magnitude, (2) quantify long-term average and seasonal trends of the contribution of groundwater to streams in the form of baseflow, and (3) evaluate the impact of climatic warming on permafrost areal extent and baseflow. A three-dimensional, transient hydrogeologic model is used to address these objectives. This model is applied to a representative headwater catchment located on the Qinghai-Tibet Plateau.

METHODS

To model groundwater flow and the effect of permafrost on baseflow we first determined the areal extent of permafrost and suprapermafrost aquifer thickness. These two permafrost parameters were computed using field measurements of surface temperature, thermal conductivity, and specific heat capacity in a one-dimensional heat conduction model that accounts for latent heat. We then input these permafrost parameters into the numerical groundwater flow model. The numerical groundwater flow model was calibrated with measurements of discharge, observations of spring locations, and hydraulic head. For a more in-depth description of the methods, please see [18].

RESULTS

Model results are examined from three perspectives. First, the steady state base case model is used as the foundation for analyzing how permafrost affects groundwater flow paths and magnitude. Second, a transient version of the base case model is employed to quantify long-term average and seasonal trends of baseflow. Third, the base model is altered to evaluate the impact of climatic warming on permafrost areal extent and baseflow contribution to streamflow.

Effect of Permafrost on Groundwater Flow

Results from the steady state simulation are depicted in Figure 2. Groundwater originates in high elevations to the south and flows toward low elevations to the north. Hydraulic head decreases with elevation. Groundwater recharges at high elevation slopes and discharges to streams.

To explore partitioning of groundwater flow in permafrost and permafrost-free regions, modeled groundwater flow was examined at three locations. Flow results will be presented from these three locations starting with the highest elevation location and proceeding downstream to the lowest elevation location.

In the high elevation permafrost region, the presence of permafrost disrupts the typical topographically controlled nested groundwater flow system (Figure 2b). In this region, 95% of the total volumetric flux, hereafter referred to as ‘‘flow,’’ is in the thin suprapermafrost aquifer. While the suprapermafrost covers more than half of the catchment surface area, with a thickness

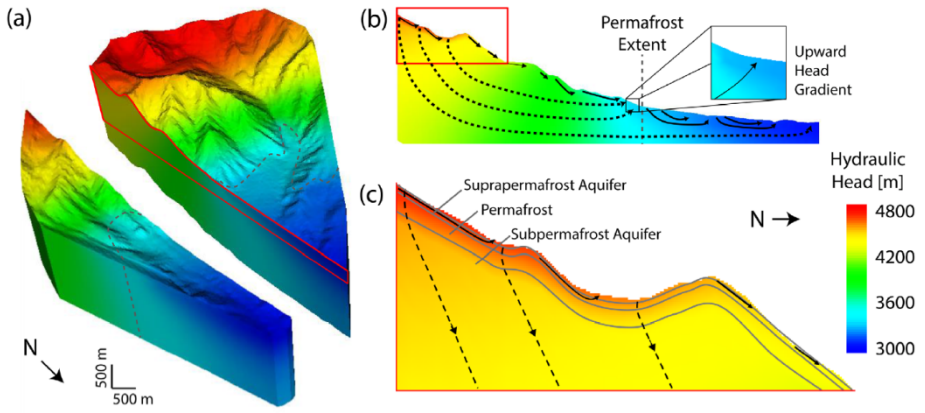

Figure 2. Modeled steady-state hydraulic head and groundwater flow paths. (a) Oblique view of the catchment showing hydraulic head. The red outline is the extent of cross section in b. (b) Cross section view of modeled head with regional and local flow lines. Flow lines, in black, are based off of flow vectors and hydraulic head. Dashed lines are flow paths with small percentages of total volumetric flux. Inset highlights upward head gradient. Red rectangle outlines the area of focus in c. (c) Detail of cross section.

of 2 m, by volume, it makes up less than one percent of the modeled catchment. Thus, the majority of flow in the permafrost region is moving through a small volume of the catchment. Only 3% of flow travels downward through the permafrost into the subpermafrost aquifer, following long, deep flow paths indicated by the dashed lines in Figure 2c.

Downstream, in the permafrost-free regions, groundwater flow systems have a typical topographically controlled nested flow pattern (Figure 2b). In this region, near the lower extent elevation of permafrost, approximately 89% of groundwater flow is concentrated in the 108 m thick surficial deposits. The remaining 11% of flow recharges into the fractured bedrock. Farther downstream, near the confluence of the Hulugou stream and Heihe River, there is increased recharge into the fractured bedrock. At this location, approximately 17% of flow recharges into the bedrock.

The influence of permafrost as a confining unit is highlighted by differences between hydraulic head in the suprapermafrost and subpermafrost aquifers. In general, hydraulic head variations are a subdued version of topography (Figure 2). There are a few areas where the subpermafrost aquifer has higher head than the suprapermafrost aquifer (e.g., Figure 2b inset). These regions with upward hydraulic head gradients are observed near the lower extent elevation of permafrost.

An upward hydraulic head gradient could drive relatively warm subpermafrost water through the permafrost to the surface. This may lead to the development of conduits or taliks. A talik is a perennially unfrozen area of the subsurface that occurs within a permafrost layer [19]. Warm groundwater from the subpermafrost aquifer can discharge through taliks leading to the development of shallow lakes and ponds [20]. This mechanism suggests a possible connection between the presence of small ponds and upwelling groundwater near the lower extent elevation of permafrost in the Hulugou catchment.

Contribution of Groundwater to Streamflow

Transient results are presented in Figure 3 which details measured precipitation, measured discharge, and modeled baseflow over one year. Results suggest that baseflow contributes ~43% of streamflow from June to November. This agrees with previous estimates that baseflow contributes 28–54% of streamflow in hydrologically similar headwater catchments (e.g., [21]).

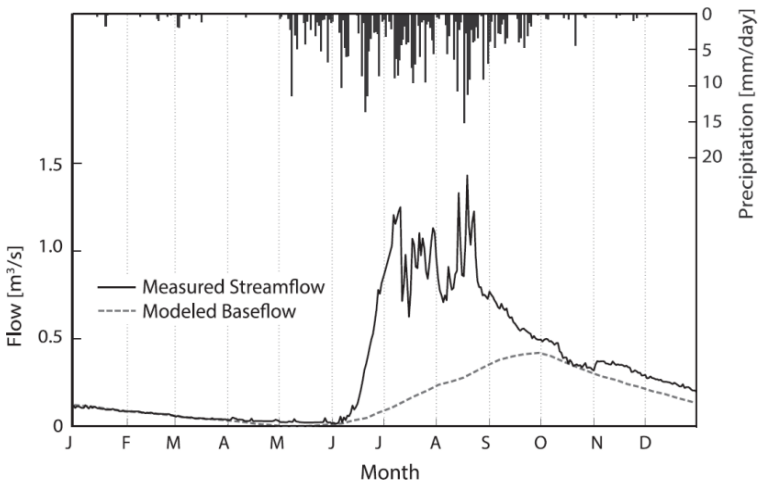

Figure 3. Hulugou catchment hydrograph. (top) Mean measured (2012–2013) daily precipitation (mm). (bottom) Mean measured (2012–2013) daily streamflow (m^3/s).and modeled weekly baseflow (m^3/s).

The transient model captures the seasonal variation of baseflow (Figure 3). Surface runoff makes up the bulk of stream discharge from late June to late August, while groundwater contribution in the form of baseflow is dominant for the rest of the year (Figure 3). Both measured stream discharge and modeled baseflow reach a minimum in early June. Measured stream discharge is highest from mid-June to late August. Discharge maximums correspond with the timing of large precipitation events. Modeled baseflow reaches a maximum in early October. The difference in timing between the maximum values of measured discharge and modeled baseflow represent the difference in the travel time of water into streams due to quick surface runoff versus slower groundwater flow. We acknowledge that our simulation of baseflow does not include seasonal freezing of the suprapermafrost aquifer and thus, slightly overestimates baseflow contribution to streamflow in the winter.

Impact of Warming on Permafrost and Groundwater Flow

In the warming scenarios, as mean annual surface temperature increases from 0 to 2°C, permafrost extent elevation increases, moving up from 3400 to 3750 m. This increase in permafrost extent elevation is equivalent to a loss in permafrost areal extent of approximately 5.5 km^2 or 28% of pre-warming

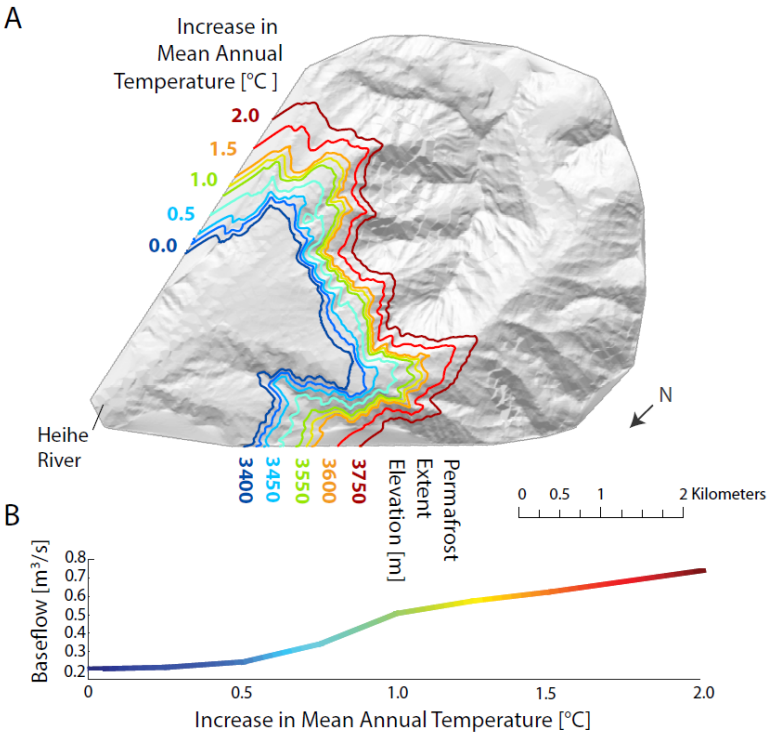

Figure 4. Effect of increasing mean annual surface temperature (°C) on (a) permafrost extent elevation (m), and (b) baseflow (m^3/s). Colors in a correspond to those in b.

permafrost area. Figure 4a illustrates the change in permafrost areal extent. In this figure, the blue line represents the permafrost extent elevation contour prior to warming and the red line shows the permafrost extent elevation contour after an increase of 2°C.

As permafrost areal extent decreases, the hydraulic conductivity of the subsurface increases, leading to increases in baseflow. Figure 4b demonstrates that as permafrost areal extent decreases, averaged baseflow increases from ~ 0.2 m^3/s to ~0.8 m^3/s. A three-fold increase in baseflow contribution to streamflow is consistent with predicted increases of baseflow under similar warming trends (e.g., [9], [19]).

CONCLUSIONS AND IMPLICATIONS

This study simulates a headwater catchment with permafrost to examine the effect of permafrost on groundwater flow and explore the response of flow to increases in mean annual surface temperature. We draw three conclusions.

First, permafrost disrupts the typical topographically controlled flow pattern observed in most headwater catchments. There is distinct flow in the suprapermafrost aquifer with a small portion of flow penetrating through the permafrost. Additionally, permafrost can act as an effective confining layer, leading to high hydraulic head in the subpermafrost aquifer with lower hydraulic head in the suprapermafrost aquifer. An upward hydraulic gradient drives warmer groundwater toward the surface promoting the creation of conduits and taliks and increasing groundwater–surface water interactions.

Second, groundwater plays a critical role in streamflow generation for headwater catchments. Groundwater contribution in the form of baseflow constitutes 43% of streamflow in the studied catchment. The presence of permafrost plays a role in this interaction as half of all flow in the catchment moves through the shallow suprapermafrost aquifer, taking short flow paths and increasing the occurrence of groundwater discharging to the surface.

Finally, an increase in mean annual surface temperature of 2°C could reduce the areal extent of permafrost, increasing groundwater discharge to streams three-fold. An increase in groundwater discharge in the suprapermafrost layer will likely promote transfer of dissolved organic carbon into the shallow subsurface.

These findings suggest that, in headwater catchments, permafrost has a large influence on groundwater flow and stream discharge, and with increased warming there will be increased groundwater discharge to streams. An increase in groundwater discharge to streams will have impacts on ecosystem health as groundwater may warm winter stream temperatures, altering stream habitat. Increases in groundwater discharge to streams, however, are only sustainable if there is adequate surface water infiltrating upstream to replenish the increased discharge downstream. If there is insufficient surface water infiltrating, there may be a lowering of the water table in the recharge area of the catchment, compromising flow downstream. A reduction in downstream flow has the potential to exacerbate seasonal freshwater deficits in lowland regions.

REFERENCES

[1] L. A. Welch and D. M. Allen, "Consistency of groundwater flow patterns in mountainous topography: Implications for valley bottom water replenishment and for defining groundwater flow boundaries," *Water Resour. Res.*, vol. 48, no. 5, May 2012.

[2] D. Viviroli, H. H. Dürr, B. Messerli, M. Meybeck, and R. Weingartner, "Mountains of the world, water towers for humanity: Typology, mapping, and global significance," *Water Resour. Res.*, vol. 43, no. 7, Jul. 2007.

[3] M. A. Walvoord and R. G. Striegl, "Increased groundwater to stream discharge from permafrost thawing in the Yukon River basin: Potential impacts on lateral export of carbon and nitrogen," *Geophys. Res. Lett.*, vol. 34, no. 12, p. L12402, Jun. 2007.

[4] W. Dobinski, "Permafrost," *Earth-Science Rev.*, vol. 108, pp. 158–169, 2011.

[5] T. Zhang, R. G. Barry, K. Knowles, F. Ling, and R. L. Armstrong, "Distribution of seasonally and perennially frozen ground in the Northern Hemisphere," in *Permafrost*, 2003, pp. 1289–1294.

[6] G. Cheng and T. Wu, "Responses of permafrost to climate change and their environmental significance, Qinghai-Tibet Plateau," *J. Geophys. Res.*, vol. 112, no. F2, p. F02S03, Jun. 2007.

[7] J. Toth, "A theoretical analysis of groundwater flow in small drainage basins," *J. Geophys. Res.*, vol. 68, no. 16, pp. 4795–4812, 1963.

[8] X.-W. Jiang, X.-S. Wang, L. Wan, and S. Ge, "An analytical study on stagnation points in nested flow systems in basins with depth-decaying hydraulic conductivity," *Water Resour. Res.*, vol. 47, no. 1, Jan. 2011.

[9] S. Ge, J. McKenzie, C. Voss, and Q. Wu, "Exchange of groundwater and surface-water mediated by permafrost response to seasonal and long term air temperature variation," *Geophys. Res. Lett.*, vol. 38, no. 14, Jul. 2011.

[10] M. T. Jorgenson, Y. L. Shur, and E. R. Pullman, "Abrupt increase in permafrost degradation in Arctic Alaska," *Geophys. Res. Lett.*, vol. 33, no. 2, p. L02503, 2006.

[11] L. Zhao, Q. Wu, S. S. Marchenko, and N. Sharkhuu, "Thermal state of permafrost and active layer in Central Asia during the international polar year," *Permafr. Periglac. Process.*, vol. 21, no. 2, pp. 198–207, Jun. 2010.

[12] G. Cheng and H. Jin, "Permafrost and groundwater on the Qinghai-Tibet Plateau and in northeast China," *Hydrogeol. J.*, vol. 21, no. 1, pp. 5–23, Dec. 2012.

[13] B. Kurylyk, K. T. B. MacQuarrie, and C. I. Voss, "Climate change impacts on the temperature and magnitude of groundwater discharge from shallow, unconfined aquifers," *Water Resour. Res.*, pp. 3253–3274, 2014.

[14] D. Guo, H. Wang, and D. Li, "A projection of permafrost degradation on the Tibetan Plateau during the 21st century," *J. Geophys. Res. Atmos.*, vol. 117, no. July 2011, pp. 1–15, 2012.

[15] V. F. Bense, G. Ferguson, and H. Kooi, "Evolution of shallow groundwater flow systems in areas of degrading permafrost," *Geophys. Res. Lett.*, vol. 36, no. 22, p. L22401, Nov. 2009.

[16] J. M. McKenzie and C. I. Voss, "Permafrost thaw in a nested groundwater-flow system," *Hydrogeol. J.*, vol. 21, no. 1, pp. 299–316, Jan. 2013.

[17] B. L. Kurylyk and K. T. B. MacQuarrie, "A new analytical solution for assessing climate change impacts on subsurface temperature," *Hydrol. Process.*, vol. 28, no. 7, pp. 3161–3172, Mar. 2014.

[18] S. G. Evans, S. Ge, and S. Liang, "Analysis of groundwater flow inmountainous, headwater catchments with permafrost," *Water Resour. Res.*, vol. 51, pp. 9127–9140, 2015.

[19] M. A. Walvoord, C. I. Voss, and T. P. Wellman, "Influence of permafrost distribution on groundwater flow in the context of climate-driven permafrost thaw: Example from Yukon Flats Basin, Alaska, United States," *Water Resour. Res.*, vol. 48, no. 7, Jul. 2012.

[20] B. J. Minsley, J. D. Abraham, B. D. Smith, J. C. Cannia, C. I. Voss, M. T. Jorgenson, M. A. Walvoord, B. K. Wylie, L. Anderson, L. B. Ball, M. Deszcz-Pan, T. P. Wellman, and T. A. Ager, "Airborne electromagnetic imaging of discontinuous permafrost," *Geophys. Res. Lett.*, vol. 39, no. 2, Jan. 2012.

[21] F. Liu, M. W. Williams, and N. Caine, "Source waters and flow paths in an alpine catchment, Colorado Front Range, United States," *Water Resour. Res.*, vol. 40, no. 9, pp. 1–16, Sep. 2004.

ASSOCIATIONS AFFECT MULTIPLE PROCESSES DURING TWO CHOICE DECISION TASKS

Christopher Mellinger

Department of Psychology and Neuroscience
University of Colorado Boulder

ABSTRACT. Responses on implicit measures of racial bias are often explained as being driven by simple associations between racial categories and stereotypic ideas. Common analysis methods such as the Process Dissociation Procedure estimate parameters reflecting this idea. However, there is theory and evidence suggesting that stereotypic responses may be driven by the effects of stereotypes on several processes in a decision making task. More advanced analyses such as the diffusion model can help to uncover such trends. In the current study, I show that performance on a common implicit measure of bias is not due to a simple monolithic association process, but is driven by effects on at least two points in the decision process: perception, and pre-existing associations. Future research to further understand these mechanisms is described, as well as implications of the work.

Contact Information: Christopher.Mellinger@colorado.edu

INTRODUCTION

Implicit measures, such as the Weapon Identification Task (WIT) and Implicit Association Task (IAT), purport to measure stereotypic associations free from social desirability effects and may even reveal unconscious associations. They have been used to study many social issues, such as gender inequality (Park, Smith, & Correll, 2010) and the recent killings of unarmed Black men (Correll, Park, Judd, & Wittenbrink, 2002). However, traditional analyses of these tasks have failed to distinguish between distinct cognitive processes that may contribute to such biases. The goal of the current research is to examine distinct processes driving racial bias through the use of advanced analysis techniques in conjunction with experimental work.

As an example, consider the WIT (Payne, 2001), in which participants must classify a target object as a gun or a nongun after seeing a face prime that varies by race. The typical finding is that classification of the object is influenced by the prime: Black faces lead participants to classify harmless tools as guns, suggesting a stereotypic association between Black men and guns. The Process Dissociation Procedure (PDP; Jacoby, 1991) can estimate participants' tendency to respond according to automatic cultural stereotypes. This tendency is estimated in a parameter called PDP-A. This is contrasted with PDP-C, which is a parameter that estimates participants' overall ability to follow task instructions. If a participant shows high estimates of PDP-C, they are showing high ability on the task. Such a participant should make few errors, but they may still show evidence that they rely on stereotypes if their PDP-A estimate is high. This indicates that the few errors they do make are in a stereotypic direction, i.e., calling tools guns after seeing Black face primes.

Based on PDP, it has been argued that automatic stereotypes drive responses toward guns after Black primes, but not after White primes. PDP-A is often treated as a monolithic mental process that reflects a drive towards stereotypical associations, as if one mental event (stereotype activation) "automatically" and directly operated on responses. But using a more complex modeling approach, I found evidence that bias in PDP-A was a product of at least two processes. Specifically, the diffusion model (Ratcliff, 1978) estimates parameters that map onto several distinct cognitive processes.

The diffusion model can be applied to many two-choice speeded-decision tasks. Figure 1 (Klauer, Voss, Schmitz, & Teige-Mocigemba, 2007) shows a diffusion model process. Decisions start at the point z. Evidence towards a particular decision is accumulated along the vertical scale in a manner specified by a random walk. In the WIT, the participant is tasked with categorizing the object on the screen as a gun or a non-gun. Thus, evidence for "gunness" is accumulated in this task. The horizontal scale is time. As time progresses, each new piece of evidence is added to the current position on the evidence scale. If evidence accumulation crosses the decision boundary a (in this case, the gun boundary), then an affirmative (gun) decision is made. If it crosses the decision boundary 0, then a negative (non-gun) decision is made. For any given set of decisions, the average rate of evidence accumulation is called the drift rate, and is represented by the parameter v. The distributions shown on the top and bottom of the graph represent reaction time distributions for the drift rate v. There is also a parameter t_0 (not depicted directly in Figure 1), which represents non-decision components of the time between stimulus onset and response, for example, the time required for a motor signal to be sent to a finger pressing a key.

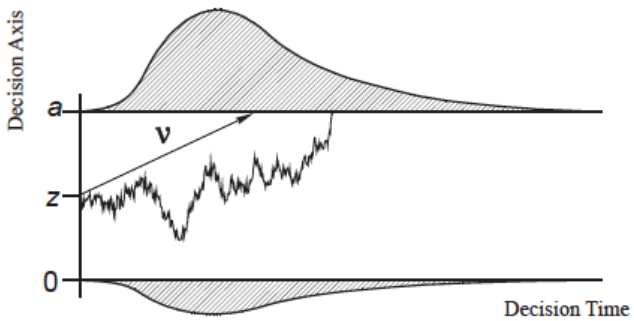

Figure 1. The Diffusion Model of Two-Choice Decisions

Two parameters in the diffusion model are of concern for the current research. *Response priming* (Voss, Rothermund, Gast, & Wentura, 2013) would suggest that seeing a face prime causes participants to form a partial response before the target object ever appears. If a participant sees a Black face, s/he may interpret the prime as evidence for a gun object because of stereotypic associations. Thus, s/he will answer more quickly and accurately if the object is in fact a gun than if it is a cell phone. The diffusion model estimates this effect as the decision starting point (the *z* parameter). In contrast, a *perceptual readiness* (Bruner, 1957) account claims that primes affect perceptual systems rather than the decision process. When a Black prime is shown, a participant's perceptual processes are prepared to respond to gun-like evidence, and less prepared for non-gun-like features. This is reflected in the drift rate parameter (*v*). It represents the speed and acuity with which evidence is accumulated from a stimulus. High drift rates indicate high perceptual ability.

The difference between these accounts can lead to very different phenomenological experiences for participants under certain conditions. Consider a situation in which a participant must make a speeded choice on the WIT, but they are given an unlimited amount of time after their initial response to correct their choice (this is of course after the stimulus has disappeared). If response priming drives bias, a participant might realize their response was incorrect after the judgment because s/he perceived the target clearly, but simply pressed the wrong key. If a change in perceptual readiness drives the mistake, participants may not even realize they made an error because they actually *perceived* (saw) a gun, *even though a tool appeared*.

In analyses of a First Person Shooter Task (Correll, 2015) (FPST), police officers showed overall less PDP-A bias than community participants. However, diffusion model analyses revealed officers actually showed *more* response priming than community participants (starting point), but were able to attenuate their bias because their perceptual expertise (drift rate) was much higher than community participants. This complex story is impossible to extract with simpler analysis methods (including PDP and other common models, such as signal detection theory or the quad-model).

Current Research

The current study reanalyzed data from a WIT. In order to examine the possible composition of PDP-A and PDP-C in terms of the diffusion model, both kinds of analysis were done on the common dataset. Then, PDP estimates were regressed on diffusion model parameters. This analysis strategy allowed the PDP estimates to be modeled as a function of diffusion processes simultaneously. Thus, different contributions from different diffusion process parameters were knowable.

METHOD

58 undergraduate students were given course credit for their participation. They completed two blocks of the WIT procedure: one practice block, and one test block. The practice block consisted of 16 trials to accustom the participants to the task. The test block consisted of 384 trials.

The WIT trials followed Payne's original procedure (2001). Each trial of the WIT began with a fixation cross. A face prime appeared, which varied by race and gender randomly across trials. The prime remained on screen for 200ms, and was replaced by a target object. The object remained on screen for 200ms, then was backward masked. If the participant did not respond within 500ms of the target onset, a message appeared telling them to go faster. For each response within the response window, feedback was provided to participants. A red X appeared if they responded incorrectly, which a green check appeared for correct responses.

RESULTS

PDP-C estimates were computed to indicate the extent to which participants were able to discriminate guns from nonguns. The mean C for objects preceded by Black primes did not differ from the mean C for White primes, $M_{difference}$=-0.01, $t(57)$=-.52, p=.61. Thus, participants were just as skillful in discriminating guns from nonguns regardless of the prime.

However, PDP-A estimates were higher (more tendency to respond gun) for Black primes than for White primes, $M_{difference}$=.22, $t(57)$=6.63, p<.001. Thus, participants were more likely to error in the direction of guns for Black primes than for White primes.

Similar tests were performed on diffusion model parameters of interest. First, drift rate were not significantly different based on prime, $M_{difference}$=-.21, $t(57)$=-.76, p=.45. This mirrors the result from PDP-C. Participants did not show perceptual skill differences based on prime. However, the race by object interaction was significant, $F(1, 57)$=24.94, p<.001. This interaction indicates that participants had higher drift rates after stereotypical prime-object pairings than after counterstereotyipcal prime-object pairings (see Figure 2). Thus, there is evidence that bias on the WIT had some basis in perceptual readiness.

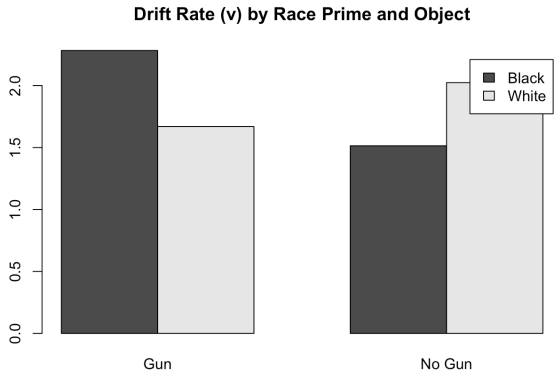

Figure 2. Drift Rate by Race Prime and Object Type

The interest of the current research was whether the bias observed in PDP-A could be accounted for with diffusion model parameters. To accomplish this, mean values of PDP-C and PDP-A, as well as race bias differences ($PDP\text{-}A_{Black} - PDP\text{-}A_{White}$, $PDP\text{-}C_{Black} - PDP\text{-}C_{White}$)

were regressed on a full set of diffusion model estimates. Each regression is depicted in Figure 3. Each column represents one model. The dependent variable (PDP estimate) is the column header, and the predictors are the row labels. The color of each box represents the *t*-value for the beta weight from that predictor. Boxes with x's are not significant. As can be seen in Figure 3, mean PDP-C correlates with the mean drift rate, showing that discriminability of guns and non-guns is dependent on fast perception. More interestingly, race bias in PDP-A is predicted by both the object by race interaction in drift rate (v), and the race bias in starting point (z). This indicates that PDP-A bias can be explained by both accounts detailed above, and is not a simple monolithic process.

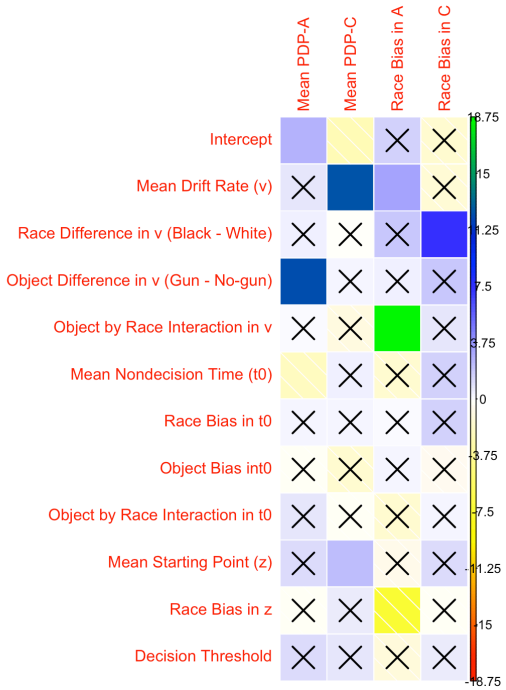

Figure 3. Regressions of PDP Estimates on Diffusion Model Parameters.

Plans for Future Research

Future research will try to better understand the core cognitive processes that underlie the so-called "automatic bias" on implicit tasks. There is an untested cognitive path from stereotypic associations to measured PDP-A bias. The re-analysis described above suggests at least two possible mediators of the link between stereotypic associations and PDP-A bias: perceptual readiness, and response-readiness. Future studies will seek to test these hypothesized mediators by manipulating them. I have already demonstrated that these distinct processes can predict PDP-A estimates through multiple-regression. In the future, I will seek to experimentally demonstrate how these distinct processes emerge and can lead to mistaken interpretations of the PDP-A parameter. Across the two studies, bias in these processes will be created by altering either the perceptual clarity of stimuli (affecting perceptual readiness), or by changing base-rate pairings (affecting response readiness). These distinct process effects should be differentially captured by diffusion model estimates, but remain indistinguishable in PDP analyses.

Implications

Parsing process-explanations of bias has important implications for the study of bias interventions, such as anti-bias police training. Several unique strategies for reducing bias have

been proposed (Payne, Shimizu, & Jacoby, 2005), and understanding low-level processes is important for evaluating them appropriately (e.g., live firearms training vs. education on stereotypic associations). More broadly, understanding the processes that contribute to race bias will importantly contribute to public discourse on this affectively charged and prominent issue.

REFERENCES

Bruner, J. S. (1957). On perceptual readiness. *Psychological Review*, *64*(2), 123–152. http://doi.org/10.1037/h0043805

Correll, J. (2015). Bias in police and community samples on the first person shooter task. *Unpublished Manuscript*.

Correll, J., Park, B., Judd, C. M., & Wittenbrink, B. (2002). The police officer's dilemma: Using ethnicity to disambiguate potentially threatening individuals. *Journal of Personality and Social Psychologycial*, *83*(6), 1314–1329. http://doi.org/10.1037/0022-3514.83.6.1314

Jacoby, L. L. (1991). A process dissociation framework: Separating automatic from intentional uses of memory. *Journal of Memory and Language*, *30*, 513–541. http://doi.org/10.1016/0749-596X(91)90025-F

Klauer, K. C., Voss, A., Schmitz, F., & Teige-Mocigemba, S. (2007). Process components of the Implicit Association Test: a diffusion-model analysis. *Journal of Personality and Social Psychology*, *93*(3), 353–368. http://doi.org/10.1037/0022-3514.93.3.353

Park, B., Smith, J. A., & Correll, J. (2010). The persistence of implicit behavioral associations for moms and dads. *Journal of Experimental Social Psychology*, *46*(5), 809–815. http://doi.org/10.1016/j.jesp.2010.04.009

Payne, B. K. (2001). Prejudice and perception: The role of automatic and controlled processes in misperceiving a weapon. *Journal of Personality and Social Psychology*, *81*(2), 181–192. http://doi.org/10.1037/0022-3514.81.2.181

Payne, B. K., Shimizu, Y., & Jacoby, L. L. (2005). Mental control and visual illusions: Toward explaining race-biased weapon misidentifications. *Journal of Experimental Social Psychology*, *41*(1), 36–47. http://doi.org/10.1016/j.jesp.2004.05.001

Ratcliff, R. (1978). A theory of memory retrieval. *Psychological Review*, *85*(2), 59–108. http://doi.org/10.1037/0033-295X.85.2.59

Voss, A., Rothermund, K., Gast, A., & Wentura, D. (2013). Cognitive Processes in Associative and Categorical Priming: A Diffusion Model Analysis. *Journal of Experimental Psychology: General*, *142*(2), 536–559. http://doi.org/10.1037/a0029459

Wittenbrink, B., & Schwarz, N. (2007). *Implicit measures of attitudes*. Guilford Press.

QUANTUM SIMULATION WITH NEUTRAL ATOMS

Roman Chapurin

JILA, NIST & the Department of Physics
University of Colorado Boulder

ABSTRACT. Classical computation and analytic approaches face many challenges when attempting to solve quantum mechanical problems. Here, I explain these difficulties and introduce quantum simulation as an alternative to attacking quantum problems. Differences between quantum simulation and quantum computation will be highlighted. Next, I focus on ultracold neutral atom systems for performing such simulations and explain experimental tools available. Lastly, I will discuss several real problems that can immediately benefit from quantum simulation.

Contact Information: Roman.Chapurin@colorado.edu

INTRODUCTION

Typical problems in physics, chemistry and other fields involve a simplified model of a real system and desire its solutions at specific times, energies, or in other limits. When equations are highly non-linear or when the model's number of degrees of freedom becomes large, exact solutions are almost impossible. While classical numerical methods advanced our understanding of various problems in many fields, they face fundamental complications when it comes to solving quantum mechanical problems.

As an example of a common quantum problem, let's consider two spin-1/2 (quantum angular momentum) particles interacting with each other. When non-interacting, each particle can be in a state spin-up $|\uparrow\rangle$ or spin-down $|\downarrow\rangle$. Generally with interactions, the two-particle composite states where both particles are spin-up $|\uparrow\uparrow\rangle$, both spin-down $|\downarrow\downarrow\rangle$, and entangled states $\frac{1}{\sqrt{2}}\left(|\downarrow\uparrow\rangle - |\uparrow\downarrow\rangle\right)$ and $\frac{1}{\sqrt{2}}(|\downarrow\uparrow\rangle + |\uparrow\downarrow\rangle)$. Therefore, the superposition of basis states $|\uparrow\uparrow\rangle$, $|\downarrow\downarrow\rangle$, $|\downarrow\uparrow\rangle$, and $|\uparrow\downarrow\rangle$ will describe this system completely for any interaction and at all times. The Hamiltonian for this system, encoding all interactions and time dependence of the two spin-1/2 particle system, is a 2x2 matrix.

A generic problem in quantum mechanics involves starting with an initial/known state at a specific time. For example, initially, the particles could be separated and be non-interacting. Then, we apply the Hamiltonian (introduce interactions) to the initial state and perform time evolution of the system. Finally, we measure the final state/solution and its properties at a particular time of interest. Note, as discussed above, that the initial and final states are written in terms of superpositions of basis states. In order to just initialize the problem and read out its solution on a computer, we need to have enough memory to store the complete basis set. In our example of the two spin-1/2 particle system we would have to store a set of $2^2 = 4$ coefficients, for N spin-1/2 particles it would be 2^N coefficients (exponential scaling). In an idealized memory, where each basis state can be represented by only one bit, we would need at least 2^{43} bits $= 1$ terabyte of memory to store information about a system of 43 spin-1/2 interacting particles. We would need more than 10^{80} bits, the estimated number of atoms in the observable universe, for 266 particles! Since our classical memory consists of bits made of multiple atoms, we clearly see limitations of classical computation in solving quantum mechanical problems with many interacting particles. Similar complications arise when the number of degrees of freedom, including the number of interaction channels, becomes large.

Multiple clever numerical algorithms were developed to solve quantum mechanical problems on a classical computer, yet, many have limitations. Certain methods, such as the mean-field based approach, only apply when interactions are weak; while others are limited to only a few particles. Even state-of-the-art quantum Monte Carlo algorithms suffer from the so-called "sign-problem", where rapidly-oscillating functions prevent sufficient convergence in numerical integration. Such functions arise due to particular symmetries and are common in strongly-interacting fermionic (e.g. electrons) and frustrated (magnetic) systems (Troyer & Wiese, 94: 170201 (2005)). While new classical numerical methods could be invented in the future, we should bet on alternative approaches.

QUANTUM COMPUTATION AND QUANTUM SIMULATION

Following pioneering work by Poplavskii (Poplavskii, 18: 222-241 (1975).), Manin (Manin, 1980), and Feynman (Feynman, 21: 467-488 (1982)) during the 1980's, the physics

community started tackling quantum problems from a different angle. Instead of trying to store quantum states on classical bits for a calculation, we can store them on intrinsically-quantum matter. This way, we won't need an exponential number of bits for storing superposition states that can be naturally encoded in quantum matter. We could use as few as N number of quantum particles to encode a state with N number of interacting particles. Now, after knowing on how to store initial and final states, two different approaches exist on how to actually perform quantum mechanical calculations: quantum computation and quantum simulation.

Quantum computation works very similar to classical computation. The initial state is written on quantum bits (qubits) made of one or several quantum elements (atoms, ions, superconducting circuits, etc.). Quantum gates, consisting of one or two qubits, perform logical operations on the state. In 1996 Lloyd showed that any unitary operation, such time evolution by a Hamiltonian, can be performed by a finite number of quantum gates (Lloyd, 273: 5278 (1996)). Therefore, we can introduce any type of interactions and dynamics we wish to our initial state. After certain time, we measure the solution to our problem by repeated measurements of our final state (quantum state tomography). While a universal quantum computer can solve any quantum problem, certain classical problems could also benefit. For example, under specific conditions, quantum annealing method can outperform its classical counterpart, simulated annealing, in finding the global minimum in optimization problems (e.g. the travelling salesman problem).

One if the biggest drawbacks of such a computer is that its efficiency is dependent on the algorithm used. For example, the prominent Trotter decomposition algorithm relies on splitting time evolution into small time steps and each step evolution is performed by a logic gate. Therefore, the calculation accuracy of dynamics of a model is directly dependent on how many gates we use. Additional complications of universal quantum computation come from the required robustness of state preparation, operations, and measurements. We need to be able to individually control and address every qubit. Likewise, quantum error correction needs to be implemented to prevent error propagation during logic operations. Currently, faced with these difficulties, universal quantum computation is many years away from realization.

Performing quantum simulations is an alternative, readily-realizable method in solving quantum problems. Quantum simulation could be thought of as a special-purpose quantum computation and sometimes referred to as analog quantum computation. That is, it cannot solve any problem like a computer can, but it can simulate certain problems. For example, often we are not interested in the exact detailed behavior of our final state, but are more interested in its collective behavior as some parameter is changed. This could be a phase transition as temperature changes or induced oscillations from sudden change in geometry. Such properties are typically robust from small imperfections and we can trust our results without needing to employ quantum error correction. These are types of problems we are trying to address in quantum simulation.

Quantum simulation works by choosing a highly-controlled physical system to imitate the physics of a real system that is hard to control or a system completely absent in nature. For example, interactions between protons and neutrons in a nucleus are not controllable but we can simulate this system by using an ultracold fermionic gas with tunable interactions (Zinner & Aksel , 40: 053101 (2013)). The Hamiltonian (dynamics and interactions) of the simulated system is being mapped onto the Hamiltonian of the simulator. During a quantum simulation the system is physically prepared in a desired state, interactions and other effects are introduced experimentally, and the system evolves to a final state that is measured.

NEUTRAL ATOMS FOR QUANTUM SIMULATIONS

There are many physical systems that are currently being used for quantum simulation, including trapped ions, superconducting circuits, quantum dots, and polar molecules (Georgescu, Ashhab, & Nori, 86: 153 (2014)). Here, I will focus on trapped ultracold neutral atomic gases. Atomic systems have many tunable experimental knobs and their sizes are easier to scale compared to others. The motion of ultracold atoms is dictated by quantum mechanics as their de-Broglie wavelengths are comparable to the interatomic spacing. Wavefunction symmetry can be selected by either using bosonic or fermionic atomic species. Trapping strength, geometry and dimensionality of these gases is controlled by their interaction with magnetic, microwave and laser fields. We can introduce periodic potentials that mimic ionic crystal lattices in solids and also employ single-lattice-site imaging and addressing. Artificial gauge fields created by sophisticated light-atom interactions and physical rotations can make neutral atoms simulate the behavior of charged particles in a magnetic field. Additionally, the interaction strength between atoms can be arbitrary adjusted by changing the magnetic field value around the so-called Feshbach resonance. Not only can these interactions be made attractive and repulsive, but also stronger than in any system existing in nature. These are just some of the exciting tools available for performing quantum simulations with neutral atoms.

PERFORMING QUANTUM SIMULATIONS

Let's look at an example of how quantum simulations help us approach quantum problems. Suppose we want to study the integer quantum Hall effect and suppose that theorists cannot explain it using analytical or classical computing methods. What we know is this effect was first observed in a semiconducting sample, surrounded by a large magnetic field, by measuring mobility properties of electrons. In order to find the underlying mechanism for this effect we will use our quantum simulator. We start off with an ideal atomic gas and will keep adding complexities (terms in the Hamiltonian) to it until we can observe the same effect. As we lower the temperature of the gas, confine it in a 2D geometry using optical traps, and introduce a large artificial magnetic field by clever light-atom interactions, we observe the integer quantum Hall effect. Additional complexities present in the real sample (including interactions, the ionic crystal lattice, fermionic or symmetry, impurities, and defects) were not needed. Performing such a quantum simulation gave us a deeper understanding of the effect's underlying physics. Going forward, we can always add the above complexities to our simulator to see what would happen to the integer quantum Hall effect. This task is very difficult, if not impossible, to do in a real sample or in a classical computer algorithm.

While the integer quantum Hall effect is well understood and can be modeled on a classical computer, there are more difficult problems where we have little understanding and classical computation made little progress. For example, high-Tc superconductivity was discovered over 30 years ago but we still lack knowledge on how it works. Having a deep understanding of high-Tc superconductivity will enable us to synthesize the revolutionary room-temperature superconductors. In my lab at JILA we use a strongly-interacting fermionic gas of uniform density to shed some light on this problem. While experimentally changing parameters, we look for evidence of atomic pairing above the critical temperature for superconductivity, believed to be the "smoking gun" of high-Tc superconductivity (Sagi, Drake, Paudel, Chapurin, & Jin, 114: 075301 (2015)).

Ultracold atomic gases could be used to simulate countless other systems in many fields including condensed matter, high-energy physics, and nuclear physics (Georgescu, Ashhab, & Nori, 86: 153 (2014)). For example, anisotropies in the cosmic microwave background (that give rise to galaxies) originating from quantum fluctuations during inflation could be simulated by Bose-Einstein condensates with propagating sound waves (Fischer & Schützhold, 70: 063615 (2004)). Likewise, three-body collinear chemical reactions can be simulated by ultracold atomic motion in a shaped waveguide (Torrontegui, Ruschhaupt, Guéry-Odelin, & Muga, 44: 195302 (2001)).

CONCLUSION

Many rich and complex quantum problems cannot be solved directly or are inaccessible to classical computation. While a universal quantum computer will be able solve any such problem, it is many years away from becoming a reality. For the time being, quantum simulations will enable us to shed light on some difficult problems.

ACKNOWLEDGEMENTS

I would like to thank STEMinar for holding intellectually-stimulating events, the NSF Graduate Fellowship Program for funding me, and my advisor Deborah Jin for inspiration.

REFERENCES

Feynman, R. P. (21: 467-488 (1982)). Simulating physics with computers. *International journal of theoretical physics*.

Fischer, U. R., & Schützhold, R. (70: 063615 (2004)). Quantum simulation of cosmic inflation in two-component Bose-Einstein condensates. *Physical Review A*.

Georgescu, I. M., Ashhab, S., & Nori, F. (86: 153 (2014)). Quantum simulation. *Reviews of Modern Physics*.

Lloyd, S. (273: 5278 (1996)). Universal Quantum Simulators. *Science*.

Manin, Y. (1980). Computable and Uncomputable. Moscow: Sovetskoye Radio.

Poplavskii, R. P. (18: 222-241 (1975).). Thermodynamic models of information processes. *(in Russian) Physics-Uspekhi*.

Sagi, Y., Drake, T. E., Paudel, R., Chapurin, R., & Jin, D. S. (114: 075301 (2015)). Breakdown of the fermi liquid description for strongly interacting fermions. *Physical review letters*.

Torrontegui, E., Ruschhaupt, A., Guéry-Odelin, D., & Muga, J. G. (44: 195302 (2001)). Torrontegui, E., et al. "Simulation of quantum collinear chemical reactions with ultracold atoms. *Journal of Physics B: Atomic, Molecular and Optical Physics*.

Troyer, M., & Wiese, U.-J. (94: 170201 (2005)). Computational complexity and fundamental limitations to fermionic quantum Monte Carlo simulations. *Physical Review Letters*.

Zinner, N. T., & Aksel , S. J. (40: 053101 (2013)). Comparing and contrasting nuclei and cold atomic gases. *Journal of Physics G: Nuclear and Particle Physics*.

PHOTOVOLTAIC APPLICATIONS OF QUANTUM DOT THIN FILMS

Alec Herr

Department of Electrical, Computer, and Energy Engineering
University of Colorado Boulder

ABSTRACT. Quantum dots (QDs) occur when the free carriers are confined in all three dimensions, and can travel only nanometers in any given direction. Being extremely small, these quantum dots contain around 10,000 to 1 million atoms each, few enough so that their energy bands form discrete levels, as opposed to the continuous bands as commonly seen in bulk semiconductors. QDs are showing promise in photovoltaics research, although the charge transport properties of common PV materials, particularly silicon, are still poorly understood. This article seeks to provide a general overview.

AUTHOR'S NOTE: This article was produced as part of the interdisciplinary 2015-16 STEMinar series. The author has not pursued original QD research in depth, but seeks to provide an overview to the interested reader.

BACKGROUND

In very small crystals, it is possible to confine particles to very small dimensions, the Heisenberg Uncertainty Principle created an uncertainty in the momentum of the particle. In bulk material, most electrons are not confined in any dimension, and are free to move throughout the material. In a quantum well, electrons are confined in one dimension, and are free to move in the other two. Similarly, quantum wires result from the confinement of electrons in two dimensions, with one dimension of free motion. [1]

In quantum dots, particles (in most cases, electrons are confined in all three dimensions, and are treated as zero-dimensional structures. As a result of such confinement, the energy of the particle at rest is increased. Because of the discrete energies of the small number of confined atoms, quantum dots behave like 'artificial atoms', as opposed to the continuous bands encountered more commonly in solids. [1] Quantum dots, as their name implies, are extremely small, with dimensions typically expressed in nanometers, and each quantum dot containing between 10,000 to 1 million atoms. [1]

The confinement of atoms in quantum dots has its benefits. In quantum dots, like individual atoms in bulk material, quantized states occur at discrete energy levels. This energy scales as $1/d^2$, where d is the diameter of the dot. [1] Therefore, electrons confined in smaller dots have higher energy. Quantum dots have only one ground state that can accommodate two electrons (spin up and spin-down, as per the Pauli Exclusion Principle). Excited states can accommodate more (two electrons in every discrete state).

MANUFACTURING

Quantum dots can be fabricated through the use of lithographic patterning (a top-down approach), or through spontaneous growth techniques (a bottom-up approach). [1]

Quantum dots can also spontaneously form in certain materials as a result of epitaxial growth and colloidal synthesis. These self-assembled quantum dots can be made using molecular beam epitaxy (MBE) or metal organic chemical vapor deposition (MOCVD). Such an example is very thin layers of one material, such as indium arsenide (InAs) deposited on a gallium arsenide (GaAs) substrate using MBE. Because of the mismatch between the lattices of the different materials used in quantum dot synthesis, it is extremely difficult to form a uniform layer that is thicker than a few atoms. This causes the surface atoms (InAs in this case) to form quantum dots on top. By depositing another layer of the substrate material (GaAs in this case), free carriers are confined in all directions. [1] The team of Chen et al at the University of Minnesota was able to achieve a silicon nanocrystal (NC) film of 180 nm in thickness. [2] These films had activation energy of around 160 meV – the energy needed to ionize such an NC. The NCs that are most easily ionized are those that contain an extra electron, which would leave behind a positive donor. [2] Despite this change of charge occurring in the NC interior, most of the charge will be found at the surface of the NC. This occurs because the dielectric constant of the interior is higher than the dielectric constant at the surface of the NC. [2]

At low levels of applied voltage, the device displays ohmic J-V characteristics. [2] In general, the conductivity of these NC films decreases as the temperature decreases. The group

Chen et al determined the relationship that conductance is proportional to Exp[-(T0/T)γ]. When γ=1, the behavior closely arises from tunneling between nearby NCs. The gamma factor can be lower with tunneling events such as Efros-Shklovskii and Mott variable-range hopping, which will not be discussed in detail here.

CHARACTERIZATION AND APPLICATIONS IN PHOTOVOLTAICS

QDs can be characterized using x-ray diffraction (CRD) or high-resolution transmission electron microscopes (HRTEM). [2] Quantum dots display similar phenomena as semiconductor nanocrystals, or NCs, which are showing promise with applications in optical electronics, such as photovoltaics and solar cells. In optical electronic devices, contacts, charge transport, and charge injection properties are important for efficient and reliable operation of these devices. [3] Much of the current research focuses on silicon, since it is non-toxic and earth-abundant. [2] Today's research seeks to understand carrier transport properties in these NC films to improve their electrical conductivity. Since solar cells operate in a wide range of temperatures, it is important to understand this effect on the carrier transport properties of silicon nanocrystals.

Another key property of these QD thin films is that their electrical properties vary with aging. Two weeks after the Chen group produced the Si NC thin films, the activation energy showed little variation, but the conductivity varied by two orders of magnitude. [2] This could arise due to change in the spacing between NCs, thus reducing the tunneling barrier. Furthermore, the absorption of water in Si QD thin films has also been widely observed. [2] The origin of the free carriers in thin films is still unknown. [2] At temperatures below 260 K, resistivity decreases with increasing temperature. In this temperature range, electron transport primarily occurs through the individual quantum states of the particles that constitute the quantum dots, rather than the surface traps. [2]

With increasing applied voltage, the activation energy of these Si NCs decreases. The Poole-Frenkel effect explains the lowering of the ionization energy due to the application of an applied electric field to the donor-containing nanocrystal. [2] With very large bias voltage, above ~16 V for the Chen group, the activation energy is even lower, and the current shows little dependence on temperature. At T=80 K, the temperature is increased by a factor of over 6 orders of magnitude as the applied voltage is increased from 1 to 16 volts. [2]

At low temperature, where T < 80 K, the observed current is nearly independent of the temperature of the nanocrystals. Because the thermal energy is so low, very few donor-containing nanocrystals receive sufficient energy for ionization. However, cold ionization processes still occur, and will in fact dominate in this low temperature range. Higher electric field implies shorter tunneling distance.

At very large electric fields (V > 16 volts), the bias voltage can generate electrons through tunneling between nearby NCs, since the voltage is sufficiently high to overcome the potential barrier and produce significant current. [2]

CONCLUSIONS

Only a small fraction of silicon NCs typically contain donor atoms, which contribute to the free current. With low applied bias, electrons travel from donor NCs to their near neighbors, and with further increase in applied bias, the carrier activation energy is reduced, and conductivity is increased. Cold ionization occurs at low temperature and high applied bias, which

is sufficient to promote tunneling with lengths on the order of 1 nm. Surface passivation is implemented to ensure that measurements are not affected by defects near the surface of the silicon NC. Many of the properties of Si NCs apply to other nanocrystalline materials as well. [2]

REFERENCES

[1] M. Fox, Optical properties of solids. New York: Oxford University Press, 2012, pp. 141-174.

[2] T. Chen, B. Skinner, W. Xie, B. Shklovskii and U. Kortshagen, "Carrier Transport in Films of Alkyl-Ligand-Terminated Silicon Nanocrystals", J. Phys. Chem. C, vol. 118, no. 34, pp. 19580-19588, 2014.

[3] K. Asadi, F. Gholamrezaie, E. Smits, P. Blom and B. Boer, "Manipulation of charge carrier injection into organic field-effect transistors by self-assembled monolayers of alkanethiols", Journal of Materials Chemistry, vol. 17, no. 19, p. 1947, 2007.

AN UPDATE ON PRESSURE SENSOR WIND SENSING WITH SMALL UAS

Roger J. Laurence III

Department of Aerospace Engineering Sciences
University of Colorado Boulder

February 15, 2016

ABSTRACT. Previously, a potential method for wind sensing with small unmanned air- craft systems (sUAS) was presented [1]. In the paper, a method of relative wind sensing involving the use of pressure sensors was discussed. Computational fluid dynamics (CFD) was used to determine suitable sensor locations from cost functions based on the change in pressure and predictability of the change. This lead to ten chosen locations near the leading edges of the wings and side plates of the Eagle Owl UAS. Some initial simulation results were also presented. Since that time, wind tunnel tests have been performed to serve as a proof of concept for this method of relative wind sensing. A 2/3 scale model of the Eagle Owl was fabricated for this test. Tygon tubing was run from the chosen sensor locations to the sensor housings that were stored off the aircraft. Results showed mean errors in the estimation of the angle of attack and sideslip of less than 1.5 degrees. Additionally, variances in the estimate of the angle of attack were lower than for sideslip. It is hypothesized that airfoils for the side plates of the Eagle Owl will lead to better estimates, as will better calibration.

Key words: unmanned aircraft, wind sensing.

Contact Information: Roger.Laurenceiii@colorado.edu

SCALE MODEL FABRICATION

For a more thorough explanation into how the sensor locations were chosen, please see [1]. With the locations chosen, fabrication of the scale model began. Fig. (1) shows the general steps for assembling the model.

After the four wing segments were completed, the tubing was installed. This involved drilling a hole from the sensor location on the surface of the airfoil to the bottom side. Trenches were then routed to allow the tubing to be flush with the underside. The segments were then combined to produce the finished top and bottom wings. A center support running towards the rear of the bottom wing was added to allow the aircraft to be mounted in the tunnel.

After the side plates were attached to the bottom wing, the top wing was then connected. A thin vertical carbon fiber spar was installed in the center of the model for structural support.

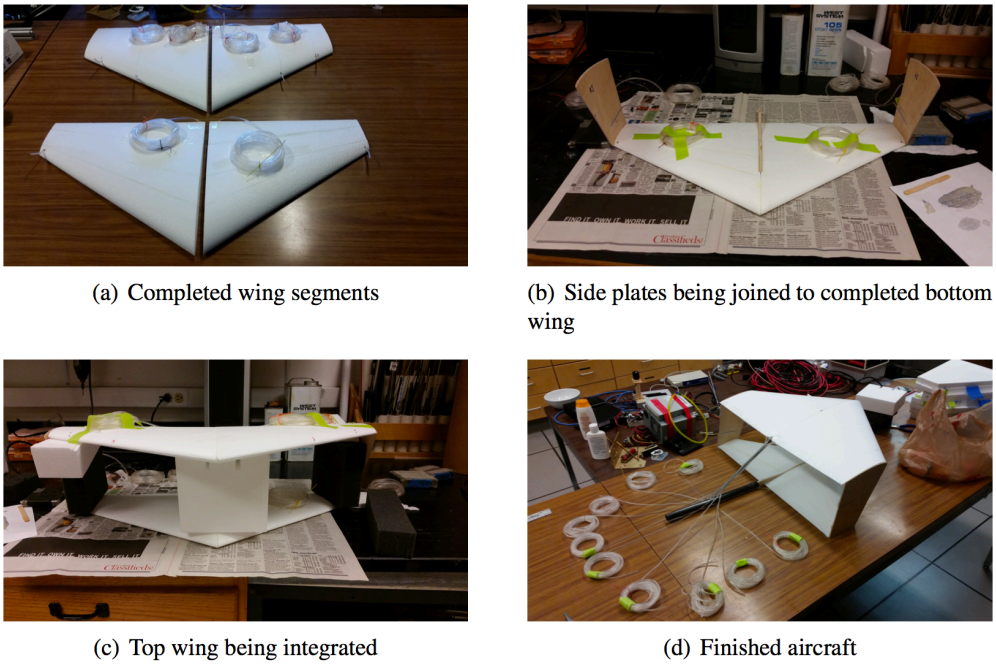

(a) Completed wing segments

(b) Side plates being joined to completed bottom wing

(c) Top wing being integrated

(d) Finished aircraft

Figure 1. Progression of the scale model assembly. The Tygon tubing shown was then connected to the pressure sensor housings.

RESULTS

Tests in the wind tunnel consisted of two phases: calibration and verification. The purpose of the calibration phase was to build up the relations between the individual sensor pressures and the angle of attack (α) and sideslip (β). The steps during the calibration phase were as follows:

1. Choose α [−4.5°, −2.5°, −0.5°, 2.0°, 3.5°, 5.5°]
2. Pre-calibration: with tunnel off, record 600 samples (28 seconds at 21 Hz)
3. Set tunnel to 10 m/s, record 600 samples per β [−5°, −3°, −1°, 1°, 3°, 5°]
4. Post-calibration: tunnel off, record 600 samples

A measurement is a reading from a single sensor; a sample is a reading from all ten sensors at the same time. Therefore, 600 samples is 6000 individual measurements. After calibration is complete, all ten sensors have 600 measurements for each of the 36 α and β pairs. These measurements are represented by the blue dots in Fig. (2). A 2 degree by 2 degree polynomial surface was fit for each sensor. The surfaces are the mathematical relationship between the pressure measurements and α and β.
With the measurement models (surface fits) acquired, the method can now be verified. The verification phase consisted of the following steps:

1. Choose α [−3.5°, −1.5°, 1.5°, 3.0°, 4.5°]
2. Calibration: with tunnel off, record 600 samples
3. Set tunnel to 10 m/s, record 600 samples per β [−4°, 0°, 4°]

Nonlinear least squares was the method chosen to estimate α and β from the measured pressures. NLS attempts to minimize the square of the residuals, as shown in the following cost function:

$$J = \frac{1}{2}[y - f(\hat{x})]^T W [y - f(\hat{x})] \tag{2.1}$$

where y are the actual pressure measurements, $\hat{x}$ is the current guess of the state variables (in this case, $x = [\alpha, \beta]^T$), $f(\hat{x})$ are the expected pressure measurements according to the surface fits and W is the weighting matrix, which is just the inverse of the sensor noise values.
15 α and β pairs were tested for verification purposes and each pair has 600 measurement samples. One sample has less total information than all 600 samples, and will lead to a less accurate estimate. The estimates from a single sample can be viewed as the worst case for estimates. For each α and β, 200 samples were randomly selected from the 600 available. NLS was performed on all 200 random samples, giving 200 estimates. Fig. (3) shows the mean values of the 200 estimates, and the standard deviations.

For the mean estimates of α, the values are all within ±1°; for β, a few mean values lie outside these bounds. The error bars around the mean values represent one standard deviation. Therefore, using only a single sample, the majority of the estimates are expected to be accurate to within 1°. This is comparable to other methods available for sUAS, yet requires a smaller financial investment and is less susceptible to damage.

FUTURE WORK

Future work involves applying this method for a flightworthy aircraft. Going forward, the airframe of choice is the Skywalker UAS, seen in Fig. (4) b. This aircraft was chosen due to the longer history of flights, and the winglets will allow for more accurate estimates of β. In addition, the larger size will allow for easy sensor installation.

The goal for the future is to be able to estimate the airspeed, V_∞, in addition to α and β. These three components will give the full relative wind speed, and will allow the design to be entirely probeless. Calibration is also going to be performed outside of a wind tunnel. A multi-hole probe will be mounted during calibration flights to match pressure measurements with relative wind measurements from the probe. Then the probe will be removed during regular flights.

During the wind tunnel tests, nonlinear least squares was used to estimate the angles α and β. Moving forward, this estimation method will be compared against other forms of nonlinear regression, such as machine learning algorithms, in an effort to determine a method that will run well onboard a low powered flight computer.

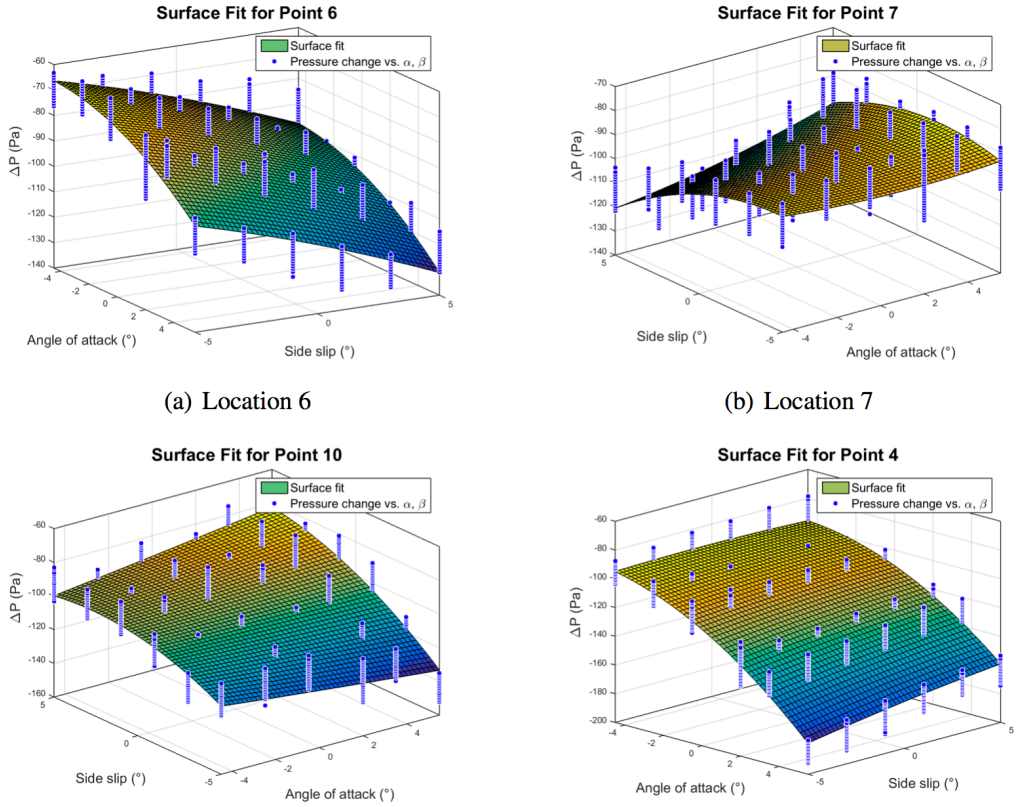

(a) Location 6 (b) Location 7

(c) Location 10 (d) Location 4

Figure 2. Surface fits showing the relation between α, β and ΔP for selected sensor locations.

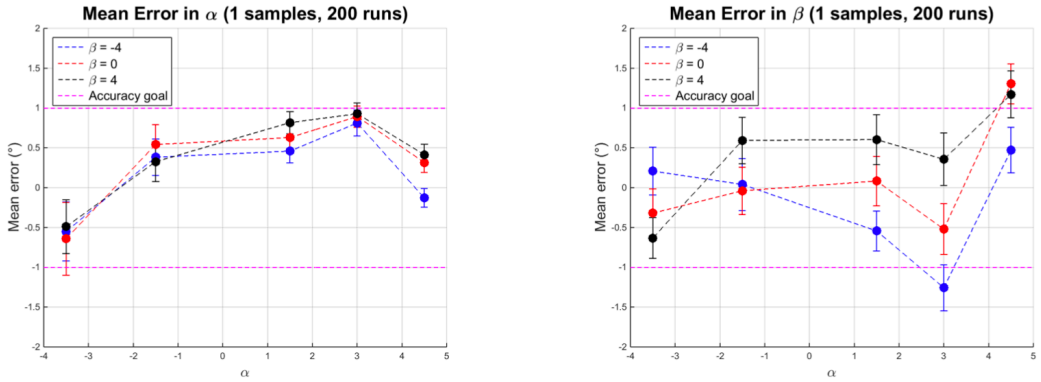

(a) Mean error in angle of attack (b) Mean error in sideslip

Figure 3. Mean errors and 1 σ error bars.

CONCLUSION

Initial wind tunnel results have shown that using pressure sensors mounted flush with the surface of the aircraft is a viable method for determining the relative wind from small unmanned aircraft. Most of the mean errors for α and $\beta \pm 1\sigma$ were less than 1° with only a single sample. However, the variances in the estimates of α noticeably smaller than for β; this can be addressed by having airfoils for the side plates. A larger aircraft will also experience a greater pressure range, thereby reducing the effect of sensor noise on the estimate.

ACKNOWLEDGMENTS

I would like to thank Trubee Davison and everyone else involved with STEMinar for all their hard work ensuring the success of the series. I would also like to thank the Graduate School for their continued support of STEMinar. I want to thank Steve Semmer of the National Center for Atmospheric Research for using the wind tunnel. Finally, I wish to acknowledge the support of my advisor Dr. Brian Argrow, along with Dr. Jack Elston, and of the Air Force Office of Scientific Research (under award no. FA9550-12-1-0412) and the National Science Foundation (under award no. AGS- 1231096) for their support of this project.

APPENDIX A. AIRCRAFT

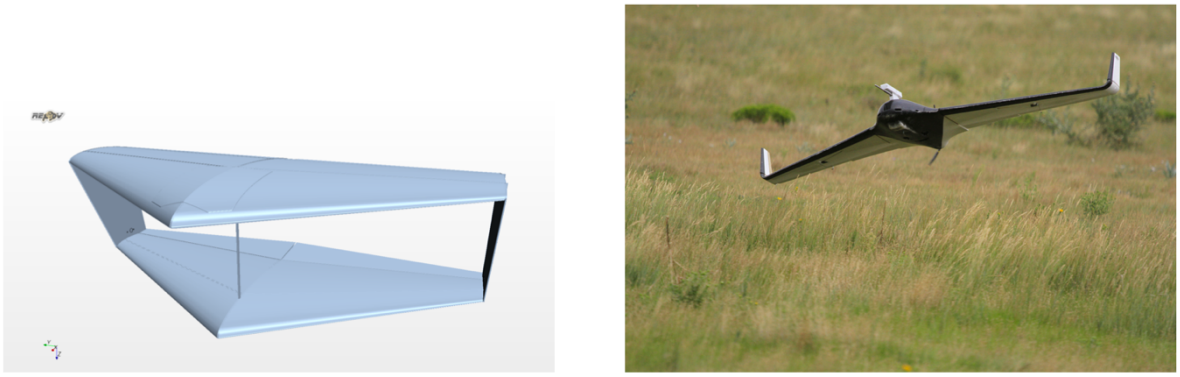

(a) CAD model of the Eagle Owl UAS (b) X-8 Skywalker about to land

Figure 4. The two aircraft currently slated to be used in this project.

REFERENCES

[1] Laurence III, R. J., "Combining CFD and Distributed Pressure Sensors for Wind Sensing with UAS", STEMinar Journal, University of Colorado Boulder, 2nd ed, pgs. 60-64, 2015, *http://www.colorado.edu/csl/sites/default/files/attached-files/stemspring.pdf*.

[2] Laurence III, R. J., Elston, J. S., and Argrow, B. M., "A Low-Cost System for Wind Field Estimation Through Sensor Networks and Aircraft Design", SciTech, Orlando, Florida, Jan 2015.

The STEMinar Team

President: Megan Harries

Megan is a fourth-year doctoral candidate in chemistry investigating the phase equilibrium of complex mixtures and developing better methods for its measurement at the National Institute of Standards and Technology. Her research interests are in the application of analytical chemistry principles and techniques to problems in energy, public health, and especially forensic science. Originally from the DC area, she studied undergraduate natural science and chemistry at Fordham University in New York. Her involvement in STEMinar is partly motivated by her desire to foster graduate student community and by her passion for science communication. She spends her free time hiking with her German Shepherd, Rocket.

Vice-President: Albany Thompson

Albany is a CU grad student in the Mathematics department. She specializes in Differential Geometry and Partial Differential Equations. With a Bachelor's of Science in Mathematics and a Bachelor's of Arts in Education from Central Washington University she is all prepared to spread the joy of STEM research wherever she goes. When she's not working, Albany likes to climb up and down tall things, expand her mental database of films, and take pictures with friendly goats.

Journal Editor: Louisa Smith

Louisa is a second-year graduate student in the Psychology and Neuroscience department. Her research focuses on the neural and genetic underpinnings of executive functions, the abilities that allow us to maintain and reach our goals. Specifically, she studies the ways in which we flexibly adapt our behavior when faced with new situations, such as a road closure on your route home. Louisa has always been passionate about increasing the accessibility of scientific research, and is excited to continue this pursuit as Editor of the STEMinar journal. Having grown up in Northern California among the redwoods, Louisa loves to spend her abundant free time exploring the Colorado mountains.